Sparse Representation of Monogenic Signal: with Application to Target Recognition in SAR Images

Ganggang Dong, Na Wang, and Gangyao Kuang, *Member, IEEE*

***Abstract*—In this letter, the classification via sparse representation of the monogenic signal is presented for target recognition in SAR images. To characterize SAR images, which have broad spectral information yet spatial localization, the monogenic signal is performed. Then an augmented monogenic feature vector is generated via uniform down-sampling, normalization and concatenation of the monogenic components. The resulting feature vector is fed into a recently developed framework, *i.e.*, sparse representation based classification (SRC). Specifically, the feature vectors of the training samples are utilized as the basis vectors to code the feature vector of the test sample as a sparse linear combination of them. The representation is obtained via ℓ_1-norm minimization, and the inference is reached according to the characteristics of the representation on reconstruction. Extensive experiments on MSTAR database demonstrate that the proposed method is robust towards noise corruption, as well as configuration and depression variations.**

***Index Terms*—Sparse representation, classification, the monogenic signal, target recognition, synthetic aperture radar.**

I. Introduction

Synthetic aperture radar (**SAR**) has been widely used in many fields due to the ability to work against inclement weather and 24-hour a day. Automatic target recognition (**ATR**) is an application of signal processing techniques to recognize the unknown targets. A typical SAR ATR system identifies the ground tactical targets through three sequential stages: detection, discrimination and classification [1], [2], and the last stage, classification, is studied in this paper.

The present techniques that devote to classification in SAR ATR include template based methods [1], model based methods [3] and the others [4], [5]. Template based methods involve extracting features and comparing with the stored templates generated by the training images. The unknown is declared as the class of the matched template. For SAR image, the matching is difficult due to the clutter background. Moreover, the variations in pose and depression increase the match complexity. Model based methods characterize the pixels in SAR image with a statistical model and then evaluate which class of parameters could maximize the posterior probability. It easily fails when there are not strong statistical relationships between the training and the testing due to the difficulty of parameter estimate under limited samples. In addition, these methods are not effective under extended operating conditions, in which the operational parameter is distinctly different between the images used for training and those used for testing.

The past several years have witnessed a great resurgence of sparse representation over a redundant dictionary. In [6], an interesting work, SRC, is reported, in which the test sample is represented in an dictionary whose base elements are the training samples themselves. With sparsity constraint, (ℓ_1-minimization), the unique representation can be generated, and the decision is made according to the residual with respect to each class. Then SRC has been extensively utilized in various classification tasks, *e.g.*, target detection and recognition [2], [7]. It is known that SAR image of a given class lie in a manifold, thus classification of SAR images is equivalent to seeking the manifold that is closest to the test image [8]. Since a manifold can be well approximated by a locally linear Euclidean space (the tangent space) [9], [10], it is applicable for sparse representation to target recognition in SAR images [2].

To make the ℓ_1-minimization computationally tractable, it is needed to reduce the data dimension. In the preceding works, both the usual features (PCA) and the unusual features (down-sampling and random projections) are verified. The results demonstrate that SRC is insensitive to the choice of feature. What is critical is whether the number of features is sufficient and whether the sparse pattern is correctly generated. As for SAR image, some issues should be further considered. First, different from the conventional optical imaging sensors, SAR image mainly results from a specular reflection rather than a diffusion one, and hence have broad spectral information yet spatial localization. Second, there are limited training resources available for target classification in SAR images. Last but not least, the standard features as recommended previously may not be effective to deal with target recognition under different poses, depression angles and configurations, because the characteristics of SAR image vary quickly and abruptly even with little changes of pose and depression, as observed from the example given in Fig.1.

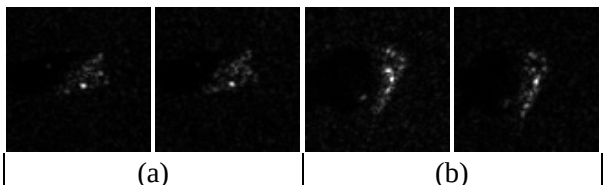

Fig. 1. SAR images (T72) with a pose change of 2° (a) and with a depression change of 2° (b); significant differences exist between each pair of SAR images.

To circumvent these problems and improve the performance,

Dr. Ganggang Dong, Dr. Na Wang, Prof. Gangyao Kuang are with the College of Electronic Science and Engineering, National University of Defense Technology, Changsha, China, 410073, e-mail: donggganggang@nudt.edu.cn, donggang.wang@gmail.com, kuangmerg@hotmail.com.

Manuscript received March 13, 2014; revised April 30, 2014.

a new classification method is proposed in this paper. The recently developed 2-D analytic signal, the monogenic signal, is adopted into SRC framework. The monogenic signal, proposed by Felsberg and Sommer [11], has been successfully used in pattern recognition, optic flow estimation, and signal processing [12]–[15]. The monogenic signal is itself a compact representation of features with little information loss and does not use steerable filters to create multi-orientation features. Moreover, it could capture the broad spectral information and spatial localization. However, the monogenic signal is infeasible to be directly applied to classification due to the high data dimension and redundancy. To circumvent the problem, this paper defines an augmented feature vector via uniform down-sampling, normalization and concatenation of the monogenic components. The resulting descriptor is then fed into SRC, and the final decision is made by searching which class of training samples could result in the minimum residual energy.

II. The Proposed Method

A. The Monogenic Signal

The analytic signal is a complex-valued representation in 1-D. Given a 1-D real valued signal $f^{(1)}(x)$, the analytic signal is defined as

$$f_a(x) = f^{(1)}(x) + if_H(x), \tag{1}$$

where $f_H(x) = -f^{(1)}(x) * \frac{1}{\pi x}$ refers to the Hilbert transformed signal. The analytic signal representation allows one to retrieve the local amplitude $A(x)$ and the local phase $\varphi(x)$

$$\begin{aligned} A(x) &= \sqrt{f^{(1)}(x)^2 + f_H(x)^2} \\ \varphi(x) &= atan2(f_H(x), f^{(1)}(x)) \end{aligned} \tag{2}$$

where $A(x)$ represents the local energy, and $\varphi(x)$ describes the local structure.

The monogenic signal is an extension of the analytic signal from 1-D to 2-D [11]. It is built around the Riesz transform, a 2-D generalization of Hilbert transform. The expression of Riesz-transformed signal in the frequency domain is $F_R(\mathbf{u}) = \frac{i\mathbf{u}}{|\mathbf{u}|}F(\mathbf{u})$, where $\mathbf{u} = (u, v)^T$ and $H(\mathbf{u}) = \frac{i\mathbf{u}}{|\mathbf{u}|}$ is the transfer function. The corresponding signal in the spatial domain is $f_R(\mathbf{z}) = -\frac{\mathbf{z}}{2\pi|\mathbf{z}|^3} * f^{(2)}(\mathbf{z})$, where $\mathbf{z} = (x, y)^T$; $f^{(2)}(\mathbf{z})$ is a 2-D signal; $*$ denote the convolution. So the Riesz kernel is $h_R(\mathbf{z}) = -\frac{\mathbf{z}}{2\pi|\mathbf{z}|^3}$.

The combination of signal $f^{(2)}(\mathbf{z})$ and its Riesz transformed one forms a 2-D analytic signal named monogenic signal,

$$f_M(\mathbf{z}) = f(\mathbf{z}) - (i, j)f_R(\mathbf{z}) \tag{3}$$

where i and j are the imagery units. As a complex number, the monogenic signal can be also described in the form of local amplitude and local phase,

$$\begin{aligned} A(\mathbf{z}) &= \sqrt{f(\mathbf{z})^2 + \|f_R(\mathbf{z})\|^2} \\ \varphi(\mathbf{z}) &= atan2(f_R(\mathbf{z}), f(\mathbf{z})). \end{aligned} \tag{4}$$

$A(\mathbf{z})$ is invariant with respect to local structure, while $\varphi(\mathbf{z})$ is invariant with respect to local energy. With the representation (3), the signal can be then represented by three components,

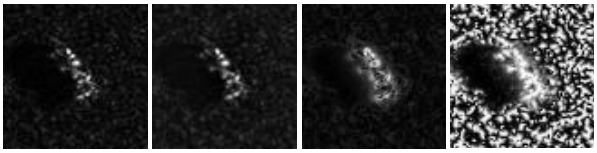

Fig. 2. Monogenic representation of SAR image (T72). (a) SAR image; (b) the real part, (c) the imagery part, (d) the instantaneous phase (cosine value).

the real part $Re\{f_M\}$, the imagery part $Im\{f_M\}$ and the instantaneous phase $\varphi(\mathbf{z})$, among which each one complements the others. Due to the wrapping phenomena, the cosine value $\cos(\varphi)$ is utilized instead of the raw phase coefficient. Example of monogenic signal is shown in Fig. 2.

Practically, the signal is of finite length, thus it is necessary to perform band-pass filtering before the Riesz transform. Here log-Gabor filters are employed due to its capability to capture broad spectral information with compact support [13], [14]. The monogenic signal can be then rewritten as

$$f_M(\mathbf{z}) = (h_{lg}(\mathbf{z}) * f(\mathbf{z})) - (i, j)(h_{lg}(\mathbf{z}) * f_R(\mathbf{z})), \tag{5}$$

where h_{lg} denote the log-Gabor kernel. Suppose S-scale log-Gabor filters are performed, the multiresolution monogenic signal can be then expressed as, $\mathbf{f} = \left[f_{M,1}, f_{M,2}, \cdots, f_{M,S}\right]$, where $f_{M,k}$ is the k-th scale monogenic signal. The raw feature tube $\mathbf{f}$ is intractable due to the high data dimension and redundancy. To cover the shortage, this paper defines an augmented feature vector via uniform down-sampling, concatenation and normalization of the monogenic components,

$$\chi_\rho(\mathbf{f}) = \left[vec(f_{M,1}); vec(f_{M,2}); ...; vec(f_{M,S})\right] \tag{6}$$

where $vec(f_{M,k}) = \left[Re_k^{(\rho)}(:); Im_k^{(\rho)}(:); P_k^{(\rho)}(:)\right]$ concatenates the column vectors of three monogenic components (*i.e.*, the real part, the imagery part, and the instantaneous phase) which are uniformly dowm-sampled by a factor of ρ.

B. Sparse Representation-based Classification (*SRC*)

Sparse representation aims to compactly recover the signal over a set of basis vectors. Given sufficient samples of k-th class, $\mathbf{X}_k = [\mathbf{x}_{k,1}, \mathbf{x}_{k,2}, ..., \mathbf{x}_{k,n_k}] \in \mathbb{R}^{m \times n_k}$, where each sample stack by its column, any new test sample $\mathbf{y} \in \mathbb{R}^m$ from the same class can be well represented with the training samples of k-th class, $\mathbf{y} = \mathbf{x}_{k,1}\alpha_{k,1} + \mathbf{x}_{k,2}\alpha_{k,2} + \cdots + \mathbf{x}_{k,n_k}\alpha_{k,n_k}$ for $\alpha_k = [\alpha_{k,1}, \alpha_{k,2}, ..., \alpha_{k,n_k}] \in \mathbb{R}^{n_k}$. Since the membership of the new sample is unknown initially, the n training samples of all K distinct classes, $\mathbf{X} = \left[\mathbf{X}_1, \mathbf{X}_2, ..., \mathbf{X}_K\right] \in \mathbb{R}^{m \times n}$, where $n = \sum_{k=1}^{K} n_k$, are used as the basis vectors. Then the linear representation of $\mathbf{y}$ can be rewritten in terms of all the training samples,

$$\mathbf{y} = \mathbf{X}_1\alpha_1 + \mathbf{X}_2\alpha_2 + \cdots + \mathbf{X}_K\alpha_K = \mathbf{X}\alpha \tag{7}$$

for $\alpha = [\alpha_1, \alpha_2, ..., \alpha_K] \in \mathbb{R}^n$. Considering the underdetermined system ($m < n$), the solution to (7) is not unique. The popular strategy is to seek the most parsimonious representation with sparsity constraint [6],

$$\min_\alpha \|\alpha\|_0 \text{ subject to } \|\mathbf{y} - \mathbf{X}\alpha\|_2 \leq \varepsilon \tag{8}$$

where $\|\cdot\|_0 : \mathbb{R}^n \mapsto \mathbb{R}$ counts the number of nonzero entries, and ε is the error tolerance. However, solving (8) in an underdetermined system is NP-hard. Thanks to the development in the theory of compressed sensing [16], if the solution $\hat{\alpha}$ is sparse enough, (8) can be relaxed as ℓ_1-norm minimization

$$\min_{\alpha} \|\alpha\|_1 \text{ subject to } \|\mathbf{y} - \mathbf{X}\alpha\|_2 \leq \varepsilon \tag{9}$$

where $\|\cdot\|_1$ sums up the absolute weights of all entries. Due to the convex property, many algorithms are presented to solve (9), as reviewed in Ref [17].

C. Sparse Representation of Monogenic Signal (*MSRC*)

Although achieving great performance previously, SRC may not be effective to deal with target recognition in SAR images, due to the distinctive characteristics, *e.g.*, broad spectral information but spatial localization. In addition, the training resources available are scarce. The monogenic signal, combination of signal and its Riesz transformation, could capture the broad spectral information and spatial localization. Moreover, its maximum bandwidth could be varied in a wide range. Thus this paper feeds the monogenic feature (6) into SRC. Specifically, the monogenic features of training samples are used as the basis vectors to represent the feature of the test sample ($\tilde{\mathbf{y}} = \chi(\mathbf{y})$) as a linear combination of them,

$$\tilde{\mathbf{y}} = \chi(\mathbf{y}) = \mathcal{D}\alpha, \tag{10}$$

where $\mathcal{D} = [\mathcal{D}_1, \mathcal{D}_2, ..., \mathcal{D}_K]$ contains the monogenic features of training samples. Here, $\mathcal{D}_k = [\chi(\mathbf{x}_{k,1}, ..., \chi(\mathbf{x}_{k,n_k})] \in \mathbb{R}^{d \times n_k}$ can be viewed as the locally linear embedding space (at the point $\tilde{\mathbf{y}}$) to approximate the manifold ($\mathcal{M}_k$) formed by the training samples of kth class.

Similar to (7), it is expected that only a small portion of atoms in $\mathcal{D}$ participate in the representation of $\tilde{\mathbf{y}}$. Thus the representation of (10) is expected to be sparse correspondingly,

$$\min_{\alpha} \|\alpha\|_1 \text{ subject to } \|\tilde{\mathbf{y}} - \mathcal{D}\alpha\|_2 \leq \varepsilon \tag{11}$$

With the sparse representation $\hat{\alpha}$, the inference is reached by evaluating which class of training samples (features) could result in the minimum reconstruction error,

$$\min_{k=1,...,K} \|\tilde{\mathbf{y}} - \mathcal{D}_k\hat{\alpha}_k\| \tag{12}$$

Actually, $\tilde{\mathbf{y}}^k = \mathcal{D}_k\hat{\alpha}_k$ can be understood as the projection of $\tilde{\mathbf{y}}$ on the subspace $\mathcal{D}_k$, and $\hat{\alpha}_k$ is the projection coefficients (weights). Then the residual $\|\tilde{\mathbf{y}} - \tilde{\mathbf{y}}^k\|$ can be regarded as the distance to the manifold $\mathcal{M}_k$. Hence the decision rule is actually to seek the minimum signal-to-manifold distance.

III. Experiments and Discussions

This section verifies the proposed method on MSTAR SAR database, a collection captured using a 10 GHz SAR sensor in one-foot resolution spotlight mode. To ensure the accuracy, two sets of experiments have been carried out, including pose, depression, and configuration variations. In the experiments, the center 80×80-pixel patch of the raw image is cropped to exclude the clutter background; the down-sampling factor in (6) is chosen from $\{\frac{1}{256}, \frac{1}{64}\}$, corresponding to the dimensions of 25D and 100D.

A. Configuration variations

Under realistic battlefield fields there may be many different physical target "configurations" that can be represented in a single target category of military significance. In the context, "configurations" simply denotes physical differences, as examples given in TABLE I.

TABLE I
Example Target Variability Categories

Variability Category	Examples
Version Variant	Smoke Grenade Launchers, Side Skits
Configuration Variant	Tow Cables, Fuel Barrels
Incidental Structural Modification	Dented Fenders, Broken Antenna Mount

This subsection considers target recognition under different configurations. All of the ten targets are utilized, and two of which, BMP2 and T72, consist of multiple variants with different configurations grouped under the same target class. The prototype configurations (SN-9563 for BMP2, SN-132 for T72) at 17° depression angle are used for training, while all the configurations at 15° depression angle are used for testing. The number of aspect views available for different targets are shown in TABLE II, where the series numbers are in bracket.

TABLE II
The number of aspect views available for different targets

	BMP2	T72	BTR70	BTR60	2S1	BRDM	D7	T62	ZIL	ZSU
17°	**233**(*9563*)	**232**(*132*)	**233**	**256**	**299**	**298**	**299**	**299**	**299**	**299**
15°	195(*9563*) 196(*9566*) 196(*c21*)	196(*132*) 195(*812*) 191(*s7*)	196	195	274	274	274	273	274	274

The recognition rates under the feature spaces of 25D and 100D are shown in TABLE III. SRC^1, SRC^2, and SRC^3 denote random projections, PCA, and down-sampling based SRC, while SVM^1 and SVM^2 stand for down-sampling and monogenic feature based SVM. To simulate the noise, we corrupt a percentage of randomly chosen pixels from the testing images, replacing their intensity with independent and identically distributed samples from a uniform distribution, as an example shown in Fig. 3. The accuracies across the level of noise are tabulated in TABLE IV. From the results of TABLE III and TABLE IV, some conclusions can be drawn:

- The accuracies for MSRC under the feature spaces of 25D and 100D are 0.8839 and 0.9366, 10.8%, 5.0%, 1.4%, and 5.04% better in average than SRC^1, SRC^2, SRC^3, and kNN. SVM^2 outperforms SVM^1 in 13.83% and 4.78% on the two feature spaces. The results prove that the monogenic feature could characterize SAR image more effectively than the holistic ones.
- The recognition rates for SRC^3 on the dimension of 25D and 100D are 0.8716 and 0.9216, compared to 0.7278 and 0.8598 for SVM^1. MSRC improves the accuracy in 1.78% and 2.99% than SVM^2. The results corroborate that SRC produces more believable inference than SVM.
- With the level of noise increased from 1% to 20%, the recognition rates of MSRC are varied from 0.9488 to 0.5726, 2.12%, 1.00%, 4.27%, 4.34%, and 11.12% better than the nearest neighbor competitor. The results show

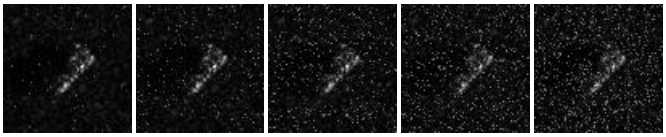

Fig. 3. Illustration of random noise corruption. The set of SAR images are of 1%, 5%, 10%, 15%, and 20% noise corruption.

that MSRC is more robust to noise corruption than the standard ones.

- The performances of MSRC consistently exceed the ones of the reference algorithms. This is because the monogenic signal, which could capture broad spectral information yet spatial localization, are adopted into SRC; hence the advantage of the monogenic signal and sparse representation are combined.

TABLE III
RECOGNITION UNDER TWO FEATURE SPACES.

Dim.	SRC^1	SRC^2	SRC^3	SVM^1	SVM^2	kNN	MSRC
25D	0.7418	0.8410	0.8716	0.7278	0.8661	0.8336	0.8839
100D	0.8620	0.8794	0.9216	0.8598	0.9067	0.8860	0.9366

TABLE IV
RECOGNITION UNDER NOISE CORRUPTION.

Noise	1%	5%	10%	15%	20%
SRC	0.9276	0.8639	0.8049	0.6419	0.4614
SVM	0.8826	0.8451	0.5310	0.4242	0.2994
kNN	0.9341	0.8579	0.8177	0.5573	0.5164
MSRC	0.9488	0.8739	0.8476	0.6853	0.5726

B. Depression Angle Variations

The second set of experiments evaluate target recognition under different depression angles. Three similar targets, 2S1, BRDM2, and ZSU23/4 are employed, as illustrated in Fig.4. Images collected at 17° depression angle are used for training, while the ones taken at 30° and 45° depressions are utilized for testing, as detailed in TABLE V. The results of the methods to be studied are shown in TABLE VI, with the confusion matrices of SRC^3, SVM^2, and MSRC drawn in Fig. 5.

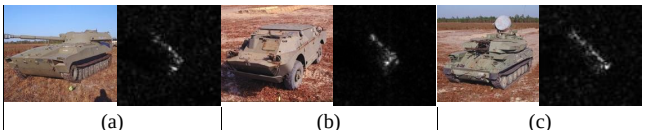

Fig. 4. Samples of 3 targets. (a) 2S1; (b) BRDM_2; (c) ZSU23/4.

As can be seen from TABLE VI and Fig. 5, it is much more challenging to recognize the targets at 45° depression than the ones at 30° depression when training the classifier with 17° depression. This is because the drastic variation in depression angle (*i.e.*, 28° versus 13°) deteriorates the data separability. The larger the variation in depression is, the more probable will it be to train the biased classifier. The phenomena is actually the over-fitting issue, an open problem still in machine learning. The performances of SVM^2 at 30° and 45° depression angles are 0.9606 and 0.5325, 3.07%, 2.92%, and 0.68% better in average than SRC^1,SRC^2 and SRC^3. The results verify that the monogenic feature could capture the characteristics of SAR image. The accuracies for MSRC at 45° and 30° depressions are 0.5963 and 0.9849, 7.48%, 7.32%, 5.08%, 8.87%, and 4.41% better in average than SRC^1, SRC^2, SRC^3, SVM^1, SVM^2. This is due to the cooperation of monogenic signal and sparse representation. Specifically, the former depicts the properties of SAR image effectively, while the latter makes the accurate inference.

TABLE V
THE NUMBER OF ASPECT VIEWS AVAILABLE FOR DEPRESSION VARIATION.

Depr.	2S1	BRDM2	ZSU23/4	SUM
training(17°)	**299**	**298**	**299**	**896**
(30°)	288	287	288	863
testing(45°)	303	303	303	909

TABLE VI
RECOGNITION RATES UNDER DEPRESSION VARIATION.

Depr.	SRC^1	SRC^2	SRC^3	SVM^1	SVM^2	kNN	MSRC
30°	0.9015	0.9166	0.9537	0.8934	0.9606	0.9525	0.9849
45°	0.5302	0.5182	0.5259	0.5105	0.5325	0.3861	0.5963

Method	Ground truth	Prediction(30°)			Prediction(45°)		
		2S1	**BRDM2**	**ZSU23/4**	**2S1**	**BRDM2**	**ZSU23/4**
SRC^{DS}	**2S1**	**271**	16	1	**123**	176	4
	BRDM2	5	**276**	6	34	**266**	3
	ZSU23/4	8	4	**276**	74	140	**89**
SVM^M	**2S1**	**260**	28	0	**63**	206	34
	BRDM2	1	**286**	0	14	**274**	15
	ZSU23/4	0	5	**283**	18	138	**147**
MSRC	**2S1**	**279**	8	1	**72**	224	7
	BRDM2	0	**287**	0	7	**294**	2
	ZSU23/4	0	4	**284**	29	97	**177**

Fig. 5. Confusion matrices of three representative methods.

IV. CONCLUSION

In this paper, the classification via sparse representation of the monogenic signal is presented, and it is applied to target recognition in SAR images. The proposed method utilize the monogenic signal to characterize SAR image, and reach the inference with sparse representation strategy. Extensive experimental comparisons of the proposed method and the standard SRC, as well as other popular algorithms (*e.g.*, NN, SVM) are conducted on MSTAR database. From these experiments, several general conclusions can be drawn as follows: the proposed method is much more robust to noise corruption, as well as various operating conditions, *e.g.*, different configurations and different depression angles, than all the reference methods. In the future, more attentions will be paid to the over-fitting issue, as shown in Section III-B.

REFERENCES

[1] L. Novak, G. Owirka, and C. Netishen, "Performance of a high-resolution polarimetric SAR automatic target recognition system," *Lincoln Lab J.*, vol. 6, no. 1, pp. 11–23, 1993.

[2] J. Thiagarajan, K. Ramamurthy, P. Knee, and *et al.*, "Sparse representation for automatic target classification in SAR images." in *Int'l Sym. Communcitaion, Control and Signal Process.*, Mar. 2010, pp. 1–4.

[3] J. O'Sullivan, M. DeVore, V. Kedia, and *et al.*, "SAR ATR performance using a conditionally gaussian model," *IEEE Trans. Aerosp. Electron. Syst.*, vol. 37, no. 1, pp. 91–108, Jan. 2001.
[4] K. Tang, X. Sun, H. Sun, and *et al.*, "A geometrical-based simulator for target recognition in high-resolution SAR images," *IEEE Geosci. Remote Sens. Lett.*, vol. 9, no. 5, pp. 958–962, Sep. 2012.
[5] M. Liu, Y. Wu, P. Zhang, and *et al.*, "SAR target configuration recognition using locality preserving property and gaussian mixture distribution," *IEEE Geosci. Remote Sens. Lett.*, vol. 10, no. 2, pp. 268–272, Mar. 2013.
[6] J. Wright, A. Yang, A. Ganesh, and *et al.*, "Robust face recognition via sparse representation," *IEEE Trans. Pattern Anal. Mach. Intell.*, vol. 31, no. 2, pp. 210–227, Feb. 2009.
[7] Y. Chen, N. M. Nasrabadi, and D. Tran, "Sparse representation for target detection in hyperspectral imagery." *IEEE J. Sel. Topics Signal Process.*, vol. 5, no. 3, pp. 629–640, 2011.
[8] V. Berisha, N. Shah, D. Waagen, and *et al.*, "Sparse manifold learning with applications to sar image classification," in *Proc. IEEE Conf. Acoustic, Sonar and Signal Processing (ICASSP)*, 2007, pp. 1081–1092.
[9] S. T. Roweis and L. K. Saul, "Nonlinear dimensionality analysis by locally linear embedding," *Science*, vol. 290, pp. 2323–2326, 2000.
[10] W. Boothby, *An Introduction to Differentiable Manifolds and Riemannian Geometry*. NY: Academic Press, 2002.
[11] M. Felsberg and G. Sommer, "The monogenic signal," *IEEE Trans. Signal Process.*, vol. 49, no. 12, pp. 3136–3144, 2001.
[12] D. Zang, L. Wietzke, C. Schmaltz, and G. Sommer, "Dense optical flow estimation from the monogenic curvature tensor," in *Proc. Int'l Conf. Scale Space and Variational Methods*, 2007, pp. 239–250.
[13] M. Yang, L. Zhang, S. Shiu, and *et al.*, "Monogenic binary coding: An efficient local feature extraction approach to face recognition," *IEEE Trans. Inf. Forensics Security*, vol. 7, no. 6, pp. 1738–1751, Dec. 2012.
[14] X. Huang, G. Zhao, W. Zheng, and M. Pietikinen, "Spatiotemporal local monogenic binary patterns for facial expression recognition," *IEEE Signal Process. Lett.*, vol. 19, no. 5, pp. 476–480, May 2012.
[15] S. C. Olhede and G. Metikas, "The monogenic wavelet transform," *IEEE Trans. Signal Process.*, vol. 59, no. 7, pp. 3426–3441, Sep. 2009.
[16] E. Candes and T. Tao, "Near-optimal signal recovery from random projections: Universal encoding strategies?" *IEEE Trans. Signal Process.*, vol. 52, no. 12, pp. 5406–5425, 2006.
[17] A. Tropp and J. Wright, "Computational methods for sparse solution of linear inverse problems," *Proc. IEEE*, vol. 98, no. 6, pp. 948–958, 2010.